Debundling of Single-Walled Nanotubes by Dilution: Observation of Large Populations of Individual Nanotubes in Amide Solvent Dispersions

ARTICLE *in* THE JOURNAL OF PHYSICAL CHEMISTRY B · SEPTEMBER 2006

Impact Factor: 3.3 · DOI: 10.1021/jp0626216 · Source: PubMed

Debundling of Single-Walled Nanotubes by Dilution: Observation of Large Populations of Individual Nanotubes in Amide Solvent Dispersions

Silvia Giordani,[†] Shane D. Bergin,[†] Valeria Nicolosi,[†] Sergei Lebedkin,[‡] Manfred M. Kappes,[‡,§] Werner J. Blau,[†] and Jonathan N. Coleman*[,†,||]

School of Physics, Trinity College Dublin, University of Dublin, Dublin 2, Ireland, Institut für Nanotechnologie, Forschungszentrum Karlsruhe, D-76021 Karlsruhe, Germany, Institut für Physikalische Chemie, Universität Karlsruhe, 76128 Karlsruhe, Germany, and Centre for Research on Adaptive Nanostructures and Nanodevices, Trinity College Dublin, University of Dublin, Dublin 2, Ireland

Received: April 28, 2006; In Final Form: June 15, 2006

Large-scale debundling of single-walled nanotubes has been demonstrated by dilution of nanotube dispersions in the solvent *N*-methyl-2-pyrrolidone (NMP). At high concentrations some very large (∼100s of micrometers) nanotube aggregates exist that can be removed by mild centrifugation. By measurement of the absorbance before and after centrifugation as a function of concentration the relative aggregate and dispersed nanotube concentrations can be monitored. No aggregates are observed below $C_{NT} \approx 0.02$ mg/mL, suggesting that this can be considered the nanotube dispersion limit in NMP. After centrifugation, the dispersions are stable against sedimentation and further aggregation for a period of weeks at least. Atomic force microscopy (AFM) studies on deposited films reveal that the bundle diameter distribution decreases dramatically as concentration is decreased. Detailed data analysis suggests the presence of an equilibrium bundle number density and that the dispersions self-arrange themselves to always remain close to the dilute/semidilute boundary. A population of individual nanotubes is always observed that increases with decreasing concentration until almost 70% of all dispersed objects are individual nanotubes at a concentration of 0.004 mg/mL. The number density of individual nanotubes peaks at a concentration of $\sim 10^{-2}$ mg/mL. Both the mass fraction and the partial concentration of individual nanotubes can also be measured and behave in similar fashion. Comparison of the number density and partial concentration also of individual nanotubes reveals that the individual nanotubes have average molar masses of ∼700 000 g/mol. The presence of individual nanotubes in NMP dispersion was confirmed by photoluminescence spectroscopy. Concentration dependence of the photoluminescence intensity confirms that the AFM measurements reflect the diameter distributions in situ. In addition, Raman spectroscopy confirms the presence of large quantities of individual nanotubes in the deposited films. Finally, the nature of the solvent properties required for dispersion are discussed.

Introduction

One-dimensional nanostructured materials such as carbon nanotubes[1] are potentially useful in a number of areas of nanoscience and nanotechnology. Single-walled carbon nanotubes (SWNTs) have mechanical,[2,3] electrical,[4] and thermal[5] properties unheard of in any other material. However, isolated SWNTs are rarely available to experimentalists. They tend to aggregate into large ropes or bundles due to their relatively high surface energy.[6] These bundles can be tens of nanometers in diameter and many micrometers long and contain huge numbers of both metallic and semiconducting SWNT tubes. Bundle properties are generally inferior to those of isolated SWNTs. It is extremely difficult to separate SWNTs from bundles making this issue a serious hurdle in the way of real applications.[3,7,8]

For this reason a number of studies have been carried out with the aim of debundling single-walled nanotubes. Most of these studies have focused on trying to disperse SWNTs down to the level of individual nanotubes in liquid-phase systems. Nanotubes have been dispersed with the aid of acids,[9,10] macromolecules,[11−14] and surfactants[15,16] as well as through covalent functionalization strategies.[17] However it has been found that dispersions consisting mainly of individual nanotubes can only be obtained at very low concentration[11] or after intense centrifugation.[16]

However, the most desirable scenario would involve the discovery of a solvent in which nanotubes are thermodynamically soluble (i.e., where the free energy of mixing is negative). Failing that, it would be advantageous to identify a solvent in which nanotubes could be dispersed down to the level of individual nanotubes or small bundles stably for reasonable periods of time. A number of reports of such solvents have appeared in recent literature.[18−25] In 1999 Liu et al. showed that individual SWNTs could be deposited from *N*,*N*-dimethylformamide (DMF) dispersions.[23] Shortly afterward Ausman et al.[18] demonstrated dispersion of SWNTs in a number of solvents including *N*-methyl-2-pyrrolidone (NMP). The authors suggest that the criteria for a successful solvent were high electron pair donicity, a low hydrogen bond donation parameter, and a high solvatochromic parameter. Bahr et al. demonstrated metastable

* Author to whom correspondence should be addressed. E-mail: colemaj@tcd.ie.
[†] School of Physics, Trinity College Dublin, University of Dublin.
[‡] Forschungszentrum Karlsruhe.
[§] Universität Karlsruhe.
[||] Centre for Research on Adaptive Nanostructures and Nanodevices, Trinity College Dublin, University of Dublin.

10.1021/jp0626216 CCC: $33.50
Published on Web 07/27/2006

dispersion of SWNTs in a range of common solvents.[19] More recently Furtado et al.[20] have shown that SWNTs can be debundled to a significant degree in both DMF and NMP. Landi et al.[22] followed this up with a quantitative study of SWNT dispersion in a range of amide solvents. In addition, Maeda et al.[24] showed that SWNTs could be dispersed in mixtures of tetrahydrofuran with various amines. However, the current authors feel that this area is important enough to warrant a more in-depth study of SWNT dispersibility in amide solvents. After a preliminary study of the dispersion properties of a range of nitrogen-containing solvents, we found NMP to be the most promising. In this paper we will focus on the dispersion of SWNTs in NMP.

In this work we use atomic force microscopy (AFM), UV−vis−NIR absorption, NIR photoluminescence, and Raman spectroscopy to show that single-walled nanotubes can be debundled simply by reducing the nanotube concentration in *N*-methyl-2-pyrrolidone dispersions. We find that the average bundle diameter decreases with decreasing concentration before saturating at approximately 2 nm below a concentration of 8×10^{-3} mg/mL. In addition a population of individual nanotubes is present at all concentrations. Furthermore the number of individual nanotubes present is maximized at a concentration of ∼0.01 mg/mL.

Experimental Procedure

Purified single-walled nanotubes (HiPCO) were purchased from Carbon Nanotechnologies, Inc., and used as supplied (lot no. PO289). Dispersions of pristine HiPCO nanotubes were prepared in *N*-methyl-2-pyrrolidone at a maximum nanotube concentration of 1 mg/mL. In general, initial dispersions were produced by sonicating for 2 min using a high-power ultrasonic tip processor, model GEX600 (120W, 60 kHz). To produce a dilution series this initial dispersion was then serially diluted to produce a range of dispersions with concentrations from 1 to 0.001 mg/mL. After each dilution the dispersions were sonicated for 2 min by tip, followed by 4 h in a low-power ultrasonic bath (Ney Ultrasonik) followed by 1 min with the sonic tip. All dispersions were subsequently centrifuged at 6000 rpm (∼4000*g*) for 90 min to remove any large aggregates. UV−vis−NIR absorption measurements were made before and after centrifugation using a Perkin-Elmer Lambda 900 UV−vis−NIR spectrometer. For comparison purposes, HiPCO SWNTs were also dispersed in an aqueous solution of sodium dodecyl benzenesulfonate (NaDDBS) (1 mg/mL HiPCO, 0.3 mg/mL NaDDBS) using an identical preparation procedure. This sample was characterized by UV−vis absorption spectroscopy and AFM.

It has been reported that sonication can damage SWNTs. To check for the presence of sonication-induced damage, Raman measurements were made on the raw SWNT powder and both the sediment and the supernatant recovered after centrifugation. Raman spectra, normalized to the intensity of the G line, were found to be almost totally identical for all three samples. No increase in the relative intensity of the D band was observed for either the sediment or the supernatant. This clearly shows that the SWNTs were not damaged by the sonication procedure.

Immediately after centrifugation a small volume from each dilution was deposited on clean silicon substrate in ambient conditions and dried at 60 °C in a vacuum oven. Atomic force microscopy studies have been carried out in tapping mode using a Multimode Nanoscope IIIA. Pointprobe silicon cantilevers (typical tip radius $R_{tip} \approx 50$ nm) were used in all cases. Due to tip size effects all lateral measurements are significantly larger than the actual object size. Because of this effect all diameter measurements were made by measuring the height of the bundle above the surface. Transmission electron microscopy (TEM) measurements were made with a Hitachi H-7000. High-resolution TEM (HRTEM) was carried out using a FEI Tecnai F20. TEM grids were prepared by placing a drop of the amide dispersion on holey carbon grids (mesh size 400).

Near-infrared photoluminescence (PL) spectra of SWNT dispersions were measured using a Bruker 66/S FTIR spectrometer equipped with a liquid-nitrogen-cooled germanium detector (sensitive in the range of ∼850−1700 nm) and a monochromatized xenon lamp excitation source as described elsewhere.[26] PL spectra were typically recorded by scanning the excitation wavelength in 3 nm steps between 550 and 900 nm and then combined into a map like that shown in Figure 9. The PL intensity was corrected using the standard procedures both for the wavelength-dependent excitation intensity and instrumental response of the spectrometer and detector (in relative photon flux units). Concentration-dependent measurements were carried out a number of times to ensure reproducibility. In all cases, the PL intensity scaled the same way with concentration. For presentation purposes the concentration-dependent PL intensity values were taken for the 1320 nm peak in the spectrum excited at 740 nm. Each set of concentration-dependent measurements were normalized to the value for the highest concentration, and then the intensity values at each concentration were averaged to give a representative concentration-dependent data set.

Raman spectra of spin-coated nanotubes on quartz substrates were acquired with a Witec CMA200 confocal Raman microscope equipped with a 100× NA 0.9 objective lens. The laser excitation wavelength, spectral resolution, and typical excitation intensity were 633 nm, ∼6 cm^{-1}, and ∼100 kW/cm^2, respectively. To localize deposited nanotubes, the substrate was scanned with a piezo table until a Raman signal was observed. The experimental procedure has been described in detail elsewhere.[27]

Results

After dilution and sonication it was observed that the higher-concentration dispersions contained significant quantities of large nanotube aggregates with sizes on the order of hundreds of micrometers. These aggregates did not appear to be present in the lower-concentration dispersions. To investigate these aggregates quantitatively, UV−vis−NIR spectra were measured for each dispersion. The dispersions were then mildly centrifuged at 6000 rpm for 90 min. After centrifugation it could clearly be seen that the aggregates had been removed. The supernatant was then carefully removed, and the UV−vis−NIR spectra were remeasured. Spectra from both before and after centrifugation are shown in Figures 1A and 1B. The relevant spectra for the NaDDBS-based dispersions are also included for comparison. In all cases absorption peaks associated with transitions between symmetric van Hove peaks in the nanotube density of states can clearly be seen. The upper axis is plotted as the reduced transition energy, n, calculated from $E = 2na_{cc}\gamma/D$ where E is the transition energy, a_{cc} is the C−C bond length (0.142 nm), γ is the C−C interaction energy ($\gamma = 3$ eV), and D is the nanotube diameter (taken as $D = 1$ nm).[22] The value of this scheme lies in the fact that the transitions near $n = 1$ are semiconductor 1−1 transitions, those near $n = 2$ are semiconductor 2−2 transitions, and those near $n = 3$ are metal 1−1 transitions.[28]

While the peaks in the absorption spectra are relatively sharp, they are not as sharp as peaks published for surfactant-dispersed

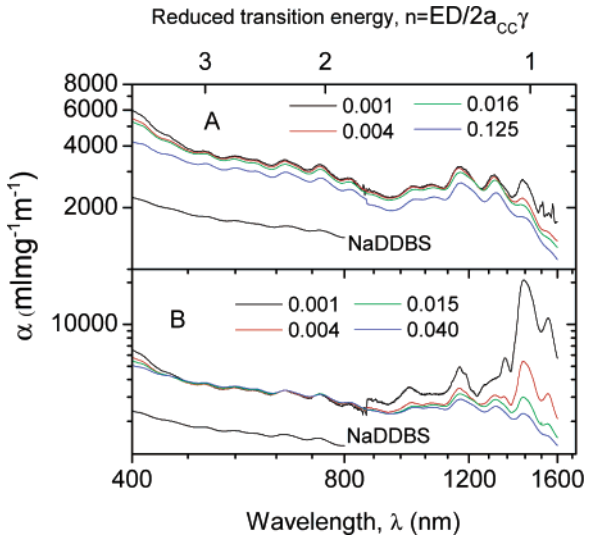

Figure 1. Absorption spectra of SWNTs dispersed in NMP at a range of concentrations (A) before and (B) after centrifugation. The concentrations (mg/mL) for both parts are given in the figure. It should be pointed out that the increase in peak height after centrifugation between 1450 and 1550 nm is probably due to slight water contamination. The upper axis represents the reduced transition energy calculated using a nanotube diameter of $D = 1$ nm, $a_{cc} = 0.142$ nm, and $\gamma = 3$ eV. Absorption spectra for dispersions of SWNTs in NaDDBS/water are shown for comparison.

SWNTs.[16] It is widely considered that the sharpness of these peaks is a measure of the level of debundling in SWNT dispersions. However, it should be pointed out that absorption spectra measured for NaDDBS-based dispersions fabricated in this study show peaks that are significantly broadened with respect to those measured for the NMP dispersions. This will be discussed further below.

The absorbance at 660 nm, A_{660}, was measured for each sample and then divided by cell length, l, to give A_{660}/l. These data are shown in Figure 2A. Before centrifugation, A_{660}/l scales approximately linearly with the initial concentration, C_I, over the whole concentration range, indicating that the aggregates at high concentration have a similar extinction coefficient to the nanotubes dispersed at low concentration. We can use the Lambert−Beer law to calculate the extinction coefficient ($\lambda =$ 660 nm) as the slope of this graph at low concentration, $\alpha_{660} =$ 3264 mL mg^{-1} m^{-1} in reasonable agreement with Landi et al. who measured values between 3000 and 3470 mL mg^{-1} m^{-1} at 700 nm for dispersions of SWNTs in various amide solvents.[22]

To further investigate the SWNT absorption coefficient, the data in Figure 2A for the precentrifuged samples were divided by the initial nanotube concentration to give a plot of α_{660} before centrifugation as a function of initial concentration as shown in Figure 2B. This graph clearly reveals variations in α_{660} as a function of concentration. At high concentrations α_{660} is relatively low, probably because the dispersions are not optically dilute in this range. At $C_I = 0.1$ mg/mL, $\alpha_{660} \approx 3250$ mL mg^{-1}m^{-1} and increases gradually, approaching 3500 mL mg^{-1} m^{-1} as C_I approaches 0.001 mg/mL. As shall be described below, this represents the range over which debundling is observed. It is possible that this increase in absorption coefficient at low concentration is associated with the increased presence of small bundles and individual nanotubes as opposed to larger bundles at higher concentrations.

After centrifugation the A_{660}/l values are significantly lower at high concentration compared to the precentrifugation measurements. This is due to the fact that the aggregates have been

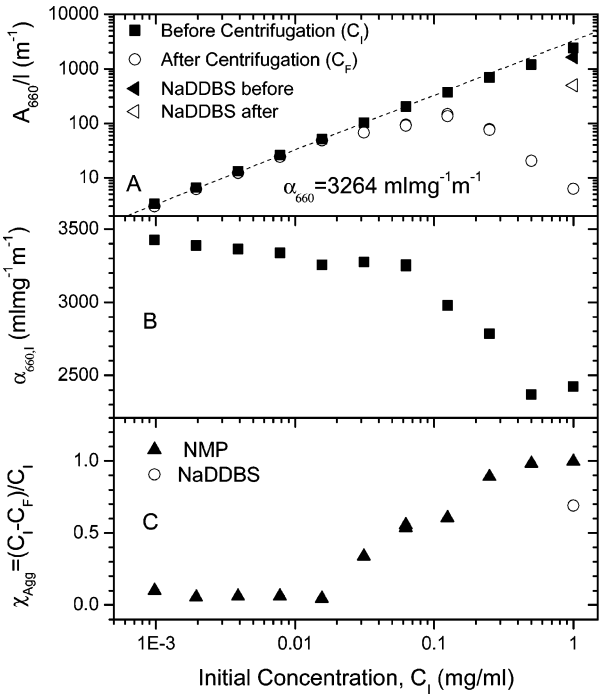

Figure 2. (A) Absorbance per unit length measured at $\lambda = 660$ nm, A_{660}/l, before and after centrifugation as a function of initial nanotube concentration. For comparison, the absorbance for a dispersion of HiPCO in NaDDBS is shown before and after centrifugation. (B) Absorption coefficient at $\lambda = 660$ nm before centrifugation found by dividing A_{660}/l by the initial nanotube concentration, C_I. (C) Fraction of the nanotube mass contained in large aggregates as a function of initial concentration.

removed by centrifugation. We can use this information in conjunction with α_{660} to calculate the new concentration after centrifugation, C_F. This concentration is the true nanotube concentration after centrifugation and shall be used exclusively from this point and referred to as C_{NT}. In addition we can calculate the mass fraction of aggregates, χ_{agg}, from

$$\chi_{agg} = \frac{A_{660,I} - A_{660,F}}{A_{660,I}} \quad (1)$$

where $A_{660,I}$ and $A_{660,F}$ are the absorbance at $\lambda = 660$ nm before and after centrifugation, respectively. This quantity is plotted in Figure 2C as a function of the initial SWNT concentration. This plot clearly shows that aggregates dominate the dispersion at concentrations above $C_I = 0.02$ mg/mL. This concentration can be thought of as the dispersion limit for SWNTs in NMP. This compares well with the dispersion limits for SWNTs in amide solvents quoted by Landi et al.[22] The observed values were between 1.6×10^{-3} and 6.3×10^{-3} mg/mL for DMF and *N*,*N*-dimethylacetamide (DMA), respectively.

In comparison, the dispersion of SWNTs in NaDDBS initially displayed an absorbance lower than the NMP sample of equivalent initial concentration (1 mg/mL) as shown in Figures 1A and 2A. However, after centrifugation the absorbance fell by approximately a factor of 3, indicating an aggregate mass fraction of 69%. It should be pointed out that this value is significantly lower than the fraction of aggregates in the NMP dispersion of equivalent concentration.

While it is well-known that SWNTs can be dispersed in NMP, it is less clear how stable these dispersions are over time. To investigate this we performed sedimentation measurements on a dispersion of SWNTs at $C_{NT} = 0.015$ mg/mL after centrifugation. This experiment involves the measurement of the sample

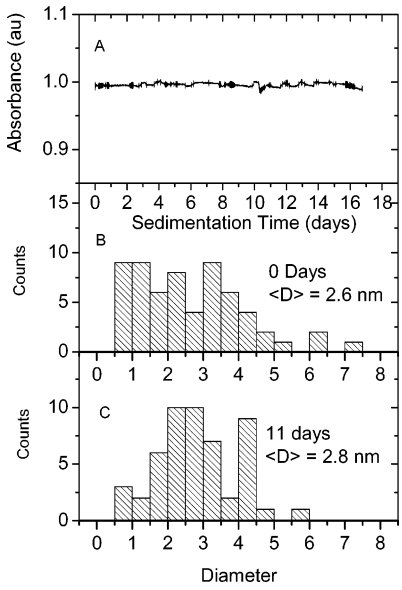

Figure 3. (A) Sedimentation curve for C_{NT} = 0.015 mg/mL after centrifugation showing stability against sedimentation. (B and C) Bundle diameter distributions for the same sample after 0 and 11 days, respectively.

absorbance (650 nm) as a function of time in a specially built apparatus,[29,30] in this case over the course of 17 days as shown in Figure 3A. The absorbance remains extremely stable over this time scale, indicating that no sedimentation occurs. However, lack of sedimentation does not necessarily mean stability. It is important to verify that no nanotube aggregation occurs over this time scale. To do this we removed a drop of the dispersion for AFM analysis immediately after centrifugation and another drop after 11 days. AFM measurements show the presence of large quantities of one-dimensional objects. In general these objects were on the order of a few nanometers high and up to 1 μm long. As the HiPCO single-walled nanotubes have diameters of 0.7−1.4 nm, the objects observed are bundles of individual tubes. The diameters of a large quantity of these bundles were ascertained by measuring their heights above the substrate. These diameters were plotted as distributions in Figures 3B and 3C and have means of 2.8 and 2.6 nm for the sample collected immediately and that collected after 11 days of sedimentation, respectively. Statistical analysis shows that these distributions are indistinguishable within a 99.99% confidence interval. This clearly shows that not only has no sedimentation occurred but that the bundles have not reaggregated over the time scale of weeks. This suggests that the dispersion is at least quasi-stable and may in fact be at or near equilibrium.

To measure the concentration dependence of the bundle size distribution, AFM measurements were also made for a set of dispersions over the entire range of concentrations. In all images large numbers of bundles were observed. Shown in Figure 4 are representative images for nanotubes at concentrations of 0.016 and 0.001 mg/mL.

It should be pointed out that, in general, reliable length distributions are difficult to obtain using AFM. This is because for samples generated from high-concentration dispersions,

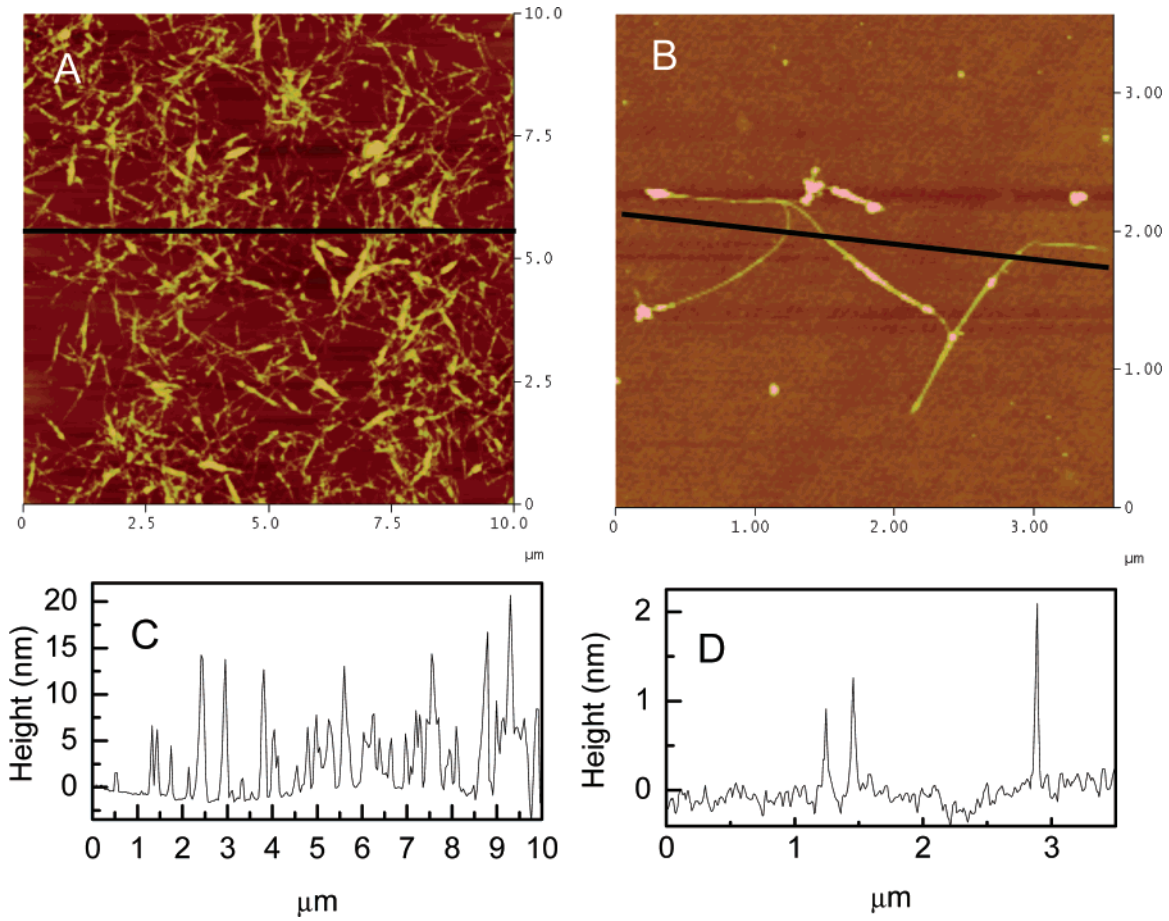

Figure 4. Typical AFM images for SWNTs at concentrations of (A) 0.016 and (B) 0.001 mg/mL. Line sections appropriate to parts A and B are shown in parts C and D, respectively. Note that the objects in part D are much smaller than the objects in part C. In part C objects with heights above 10 nm are due to the intersection of bundles that cross each other.

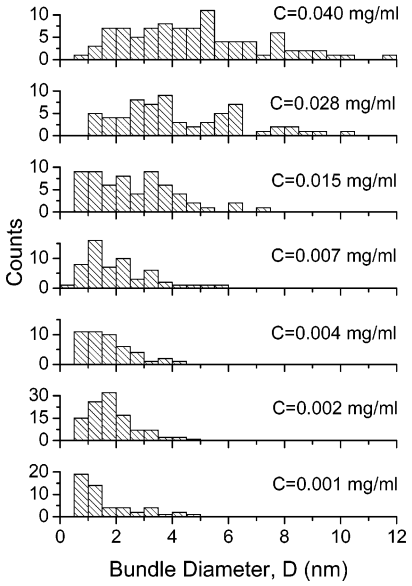

Figure 5. Histograms of bundle diameters for SWNTs dispersed in NMP at a range of concentrations from 0.04 to 0.001 mg/mL. Diameters were measured from AFM images of material deposited from the dispersion immediately after sonication. Decreases in concentration are accompanied by a downshift of the diameter distribution. Note that a population of single, isolated nanotubes is present at all concentrations.

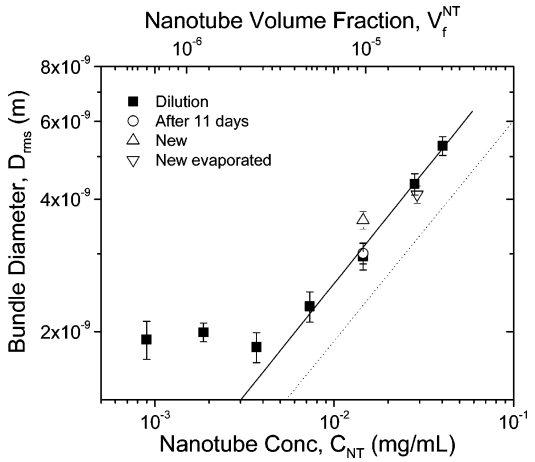

Figure 6. Diameters of nanotube bundles as a function of concentration as obtained from the diameter distributions (labeled "dilution"). This is plotted as the root-mean-square diameter to facilitate analysis using eq 2. The error bars are calculated from the standard error of the distribution. The root-mean-square bundle diameter decreases with decreasing concentration before saturating at approximately 1.9 nm. The solid line comes from fitting eqs 4 and 5. The dotted line is calculated from eq 5 assuming that each bundle occupies exactly its own spherical volume with $L_{bun} = 900$ nm. The open circle shows the diameter measured after 11 days. The up triangle labeled "new" represents the dispersion made up directly at 0.015 mg/mL while the down triangle labeled "new evaporated" represents the bundle diameter of this sample after evaporation.

completely isolated objects are rare and it can be difficult to determine the positions of the ends of a given bundle. However, the bundle length could be measured by TEM for the $C_{NT} = 0.024$ mg/mL sample giving a value of $L_{bun} = 900 \pm 270$ nm. The average length of the individual nanotubes could be measured from the low-concentration AFM images to be $L_{NT} = 785 \pm 70$ nm (accounting for tip effects). It is interesting that these two values are equal within error. This suggests that the nanotubes in small bundles rearrange themselves to maximize their (negative) binding energy as suggested previously by Nicolosi et al.[29]

It is much more straightforward to measure bundle diameters even for samples containing criss-crossing bundles. In addition, as the bundle and individual nanotube lengths are equal within error, most of the bundle size information is contained in the diameter distribution. Thus, to investigate the size distribution of the bundles, diameter measurements were made for all bundles observed in the AFM images. These were then plotted as diameter distributions for each concentration. These diameter distributions are shown in Figure 5.

From Figure 5 it can clearly be seen that the bundle diameters shift to lower values as the concentration is decreased. In fact at the lowest concentration studied (10^{-3} mg/mL), almost 75% of bundles had diameters of less than 2 nm. In addition it can be seen that a significant population of small bundles with $D < 2$ nm exists at *all* concentrations.

The root-mean-square bundle diameter, $D_{rms} = \sqrt{\langle D^2 \rangle}$, as a function of concentration is shown in Figure 6. For completeness the top axis also shows the concentration transformed into the nanotube volume fraction, V_f^{NT}, using $V_f^{NT} = C_{NT}/\rho_{NT}$ where ρ_{NT} is the nanotube density ($\sim$1500 kg/m^3).[31] The root-mean-square diameters tend to fall monotonically from approximately 6 nm at high concentration to less than 2 nm at $C_{NT} = 0.008$ mg/mL before saturating at this level. This sort of debundling phenomenon has been previously observed for SWNT−polymer dispersions[11] and for inorganic nanowire dispersions.[29] For comparison purposes the NaDDBS−SWNT dispersion ($C_{NT} = 0.31$ mg/mL) was measured to have $D_{rms} = 5.3 \pm 0.6$ nm, which is comparable to the bundle size measured for the high-concentration NMP dispersions.

This apparent dependence of bundle diameter on concentration has a number of possible explanations. One possibility is the formation of an anisotropic nanotube phase in solution due to concentration-dependent steric effects. This could result in concentration-dependent aggregation of the aligned nanotubes. Both Onsager and Flory calculated that such an anisotropic phase is stable only above a minimum volume fraction V_f^{min}, which depends on the aspect ratio, x[32]

$$V_f^{min}(x) = \frac{8}{x}\left(1 - \frac{2}{x}\right) \tag{2}$$

At the highest concentration studied ($C_{NT} = 0.04$ mg/mL, $V_f^{NW} \approx 2.67 \times 10^{-5}$) the average bundle dimensions (quoted above) result in aspect ratios of 170 and hence values of V_f^{min} of 0.05. This value of V_f^{min} is far above the concentration range studied, which means that all our nanotube dispersions are expected to be isotropic. Thus steric effects are unlikely to be responsible.

Another possibility is due to the fact that during the serial dilution the dispersions underwent successively longer sonication with each sequential dilution. It is possible that this could result in debundling due to increased sonication and not due to reduced concentration. To test this we made up a dispersion directly at 0.015 mg/mL. This dispersion received significantly less sonication than the original 0.015 mg/mL sample prepared by dilution. The root-mean-square bundle diameter from this sample is shown on Figure 6. This datum is close to the previous measurement within error showing that different sonication times do not lead to significantly different levels of debundling.

To confirm that the bundle diameter is actually controlled by concentration, we allowed the solvent to evaporate from the new 0.015 mg/mL sample resulting in an increase in concentration. Measurements of the bundle diameter distribution were made after enough NMP had evaporated to give a concentration of 0.03 mg/mL. The bundle diameter distributions were

measured, and the D_{rms} values are plotted in Figure 6. The bundle diameters measured during this evaporation experiment are identical to those measured for equivalent concentrations during the dilution experiment. This strongly suggests that the bundle diameter distribution evolves to an equilibrium value that is controlled by nanotube concentration.

We can model the concentration dependence of the debundling process very crudely by noting that the input of sonic energy tends to drive the system toward debundling. However, as debundling occurs the dispersion becomes dominated by large quantities of small bundles. This increases the probability of aggregation. This suggests that a quasi-equilibrium will be reached. We suggest that this equilibrium state is characterized by an equilibrium number density of bundles. This is equivalent to an equilibrium volume of solvent per bundle. In this case we can easily write this equilibrium number density $(N/V)_{eq}$ in terms of the equilibrium (average) bundle volume $\langle V_{bun}\rangle$

$$\left(\frac{N}{V}\right)_{eq} = \frac{C_{NT}}{\rho_{NT}\langle V_{bun}\rangle} \tag{3}$$

where C_{NT} is the mass concentration of nanotubes and ρ_{NT} is the nanotube density. We should note that while we do not know how the average bundle volume scales with concentration we have measured how the bundle diameter scales with concentration. If we approximate the bundle length (L_{bun}) as constant, then we can rearrange to obtain

$$D_{rms} = \sqrt{\langle D^2\rangle} \approx \left[\frac{4C_{NT}}{\rho_{NT}\pi L_{bun}(N/V)_{eq}}\right]^{1/2} \tag{4}$$

This expression has been fitted to the data in Figure 6 (solid line) and represents a very good fit. Taking $\rho_{NT} = 1500$ kg/m^3 and using the value for nanotube length obtained from TEM, we can calculate the equilibrium bundle number density. This was calculated to be $(N/V)_{eq} = (1.5 \pm 0.6) \times 10^{18}$ m^{-3}. Taking the inverse of this quantity gives the equilibrium solvent volume per bundle, V_{sol}^{eq}. This volume can be considered similar to the pervaded volume concept used in polymer physics.[33] This can be calculated at $V_{sol}^{eq} = (6.7 \pm 2.7) \times 10^{-19}$ m^3. Interestingly, this volume is close to the volume of a sphere whose diameter is defined by the average bundle length (900 nm). The volume of this sphere is $V_{sphere} = (3.8 \pm 3.4) \times 10^{-19}$ m^3. If we consider V_{sphere} as the volume of solvent occupied by the nanotube, then, in this case, each bundle on average almost exactly occupies its own pervaded volume. In polymer physics terminology this occurs at the overlap concentration. Interestingly nanotubes dispersed in NMP appear to adjust their bundle size distribution with concentration to always be close to the overlap concentration.

Each bundle occupies exactly its own pervaded volume when $V_{sol}^{eq} = V_{sphere}$. We can easily show that if this is the case then

$$D_{rms} = L_{bun}\sqrt{\frac{2}{3}\frac{C_{NT}}{\rho_{NT}}} = L_{bun}\sqrt{\frac{2}{3}V_f} \tag{5}$$

Taking $L_{bun} = 900$ nm and with $\rho_{NT} = 1500$ kg/m^3 we can plot D_{rms} in this scenario as the dotted line in Figure 6. This curve matches qualitatively to the experimental data for D_{rms}. The fact that the bundles have slightly larger diameters than those predicted by this model suggests that in reality $V_{sol}^{eq} > V_{sphere}$. Alternatively we can assume that the bundles exactly occupy their own pervaded volume and fit eq 5 to the data in Figure 6 (solid line). We can then calculate L_{bun} from the fit. This works out to be $L_{bun} = 1275 \pm 250$ nm, slightly larger than that measured by TEM. It is not clear which of these scenarios is closer to reality.

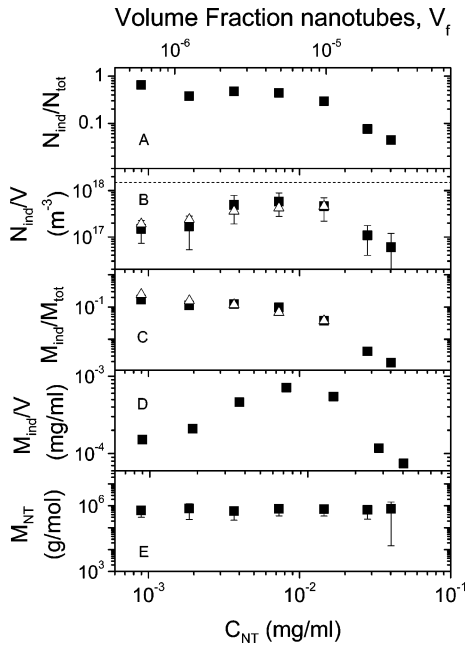

Figure 7. (A) Number fraction of individual nanotubes as a function of concentration as obtained from the diameter distributions. (B) Number of individual nanotubes per unit volume. (C) Mass fraction of individual nanotubes. (D) Partial concentration of individual nanotubes. (E) Molar mass of individual nanotubes as calculated from the data presented in parts B and D. The data represented by open triangles in parts B and C are derived from photoluminescence data.

In polymer physics, concentrations below the overlap concentration are considered dilute, and interchain interactions can be neglected. The fact that $V_{sol}^{eq} > V_{sphere}$ then suggests that the dispersions are balanced slightly below the dilute/nondilute interface (using the value for L_{bun} as measured by TEM). In this situation aggregation may be limited by random collisions between bundles. If each bundle is the sole occupier of its own spherical volume, then collision cannot occur due to random rotations (tumbling) of adjacent bundles. Collisions are then rare as they can only occur due to translational diffusion, which for nanotubes is a slow process.

This clearly suggests that the bundle size is related to the equilibrium number density. In turn this means that bundle dimensions can be related to nanotube concentration simply by considering the volume of the sphere traced out by the tips of the bundle as it tumbles through the solution. This is potentially an important tool for planning concentrations in dispersions of one-dimensional nanostructured materials.

It is known that the individual HiPCO SWNTs have diameters in the range 0.7−1.4 nm. This suggests that any object observed with a height of ≤1.4 nm is probably an individual nanotube although it may be a small bundle of 2 or 3 nanotubes lying flat. We can calculate, from the diameter distributions, the ratio of individual tubes to the total number of objects, N_{ind}/N_T. This quantity is shown in Figure 7A and increases as concentration decreases, from ∼5% at $C_{NT} = 0.04$ mg/mL to nearly 70% at $C_{NT} = 0.004$ mg/mL. This shows that 70% of the objects at low concentration are individual nanotubes. This compares to measurements by Furtado et al. on dispersions of acid-treated nanotubes in DMF and NMP where 50−90% of objects are individual nanotubes.[20] The presence of large quantities of individual SWNTs in low-concentration NMP dispersions was

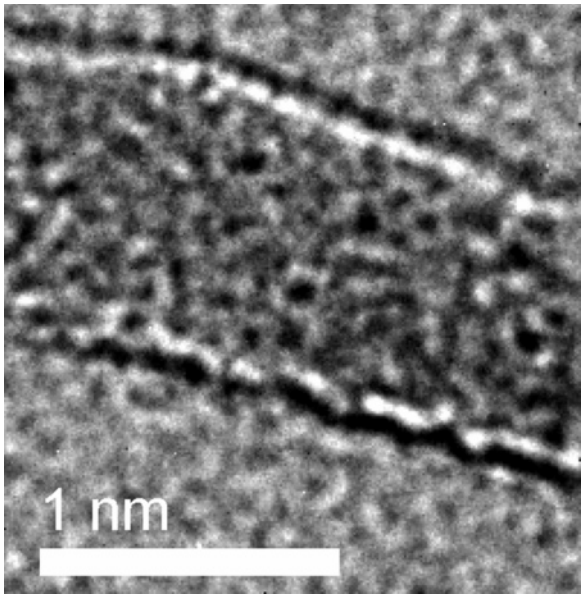

Figure 8. Close up HRTEM image of an individual SWNT. Sample prepared from a dispersion with concentration $C_{NT} = 0.001$ mg/mL.

confirmed by HRTEM studies. HRTEM measurements were made on the $C_{NT} = 0.001$ mg/mL sample. While small bundles of diameters of 2−3 nm were observed the sample was dominated by individual SWNTs, confirming the AFM measurements. A HRTEM image of an individual SWNT is shown in Figure 8.

In addition we measured N_{ind}/N_T for SWNTs dispersed using NaDDBS ($C_{NT} = 0.31$ mg/mL) to be 17%, significantly higher than the values for high-concentration NMP dispersions. This leads to an interesting observation. The fraction of individual nanotubes is higher in the NaDDBS dispersion (17%) compared to that in the high-concentration NMP dispersions (5% for $C_{NT} = 0.04$ mg/mL). However, as shown in Figure 1 the absorption peaks are actually sharper for the $C_{NT} = 0.04$ mg/mL NMP dispersion. This clearly shows that absorption peak width does not necessarily correlate with the level of debundling as is generally thought. It is probable that the interaction between the nanotube and the dispersing medium can have a significant effect on the peak width. In some cases this may in fact outweigh the contribution due to internanotube interaction (or lack of).

We can use the data on the fraction of individual nanotubes to calculate the absolute number of individual nanotubes per unit volume of solvent by noting

$$\frac{N_{ind}}{V} = \frac{N_{ind}}{N_T}\frac{N_T}{V} \approx \frac{N_{ind}}{N_T}\frac{4C_{NT}}{\rho_{NT}\pi\langle D^2\rangle L_{bun}} \tag{6}$$

where all symbols have the same meaning as before. The number density has been calculated and is shown in Figure 7B. For HiPCO SWNTs dispersed in NMP the number density of individual nanotubes peaks around $C_{NT} = 0.01$ mg/mL. This shows unambiguously that even as the concentration decreases the number of individual nanotubes can increase if the debundling process is efficient enough. Also shown as the dashed line in Figure 7B are values of $(N/V)_{eq}$ calculated earlier. It is clear that the maximum number of individual tubes per volume approaches the equilibrium bundle number density. This shows that $(N/V)_{eq}$ can be thought of as a maximum bundle number density.

In addition we can estimate the mass fraction of individual nanotubes from the diameter distributions. Assuming the densities of bundle and individual nanotubes are equal and given that the bundle length and the individual tube length are equal within error, we can write

$$\frac{M_{ind}}{M_T} = \frac{\sum_{D<1.4\text{nm}} D^2 L_{ind}}{\sum D^2 L_{bun}} \approx \frac{\sum_{D<1.4\text{nm}} D^2}{\sum D^2} \tag{7}$$

This quantity has been calculated and is presented in Figure 7C. The mass fraction of individual tubes increases with decreasing concentration, saturating at approximately 20%. This saturation value is of course less than that for the number density of individual tubes (Figure 7B) as much of the mass is concentrated in the larger bundles.

We can use these data to calculate the mass of individual nanotubes per unit volume of solvent, M_{ind}/V. This can be thought of as a partial concentration of individual nanotubes. We can calculate this using the fact that

$$\frac{M_{ind}}{V} = \frac{M_{ind}}{M_T}\frac{M_T}{V} = \frac{M_{ind}}{M_T}C_{NT} \tag{8}$$

This quantity has been calculated and is presented in Figure 7D. These data are very similar to that presented in Figure 7B, increasing as concentration decreases to a maximum of $(M_{ind}/V) \approx 8 \times 10^{-4}$ mg/mL at total concentrations of $C_{NT} \approx 8 \times 10^{-3}$ mg/mL. Interestingly enough, both N_{ind}/V and M_{ind}/V display maxima around 8×10^{-3} mg/mL. These concentrations represent the conditions under which the total number of individual tubes is maximized. This is an unexpected result. One might naively assume that the number density of individual tubes might be maximized at high concentration or at a low concentration where all the objects are individual tubes. However the fact that the number of individual tubes is maximized at a midrange concentration where the individual tubes coexist with a population of bundles is extremely interesting.

The ratio of M_{ind}/V to N_{ind}/V is just the average mass per nanotube. As these two quantities, as presented in Figures 7B and 7D, are calculated in different manners we can use their ratio to calculate the average nanotube mass. This is plotted as a function of concentration in Figure 7E as the nanotube molar mass. This value is invariant with concentration as would be expected. The average of these values is 6.8×10^5 g/mol.

We have been able to derive much information about the system from AFM studies of deposited bundles. However, the possibility still remains that the concentration dependence of the bundle size distributions is actually dominated by drying effects. In fact, theoretical studies have shown that concentration-dependent bundling effects can actually occur for one-dimensional objects that are mobile during drying.[34] To rule this possibility out we need an in situ measurement technique that gives information about either the bundle size distribution or alternatively the population of individual nanotubes. Such a technique is infrared photoluminescence, which is sensitive only to individual nanotubes.

Near-infrared PL measurements were made on a number of concentrations of SWNTs in NMP. Shown in Figure 9a is a typical photoluminescence map measured for one of our dispersions. The PL provides additional strong evidence for the presence of a significant fraction of individual nanotubes in NMP dispersions, since the PL is almost completely quenched in large bundles of SWNTs.[16] In comparison to water−surfactant dispersions of HiPCO nanotubes (Figure 9B), PL peaks are

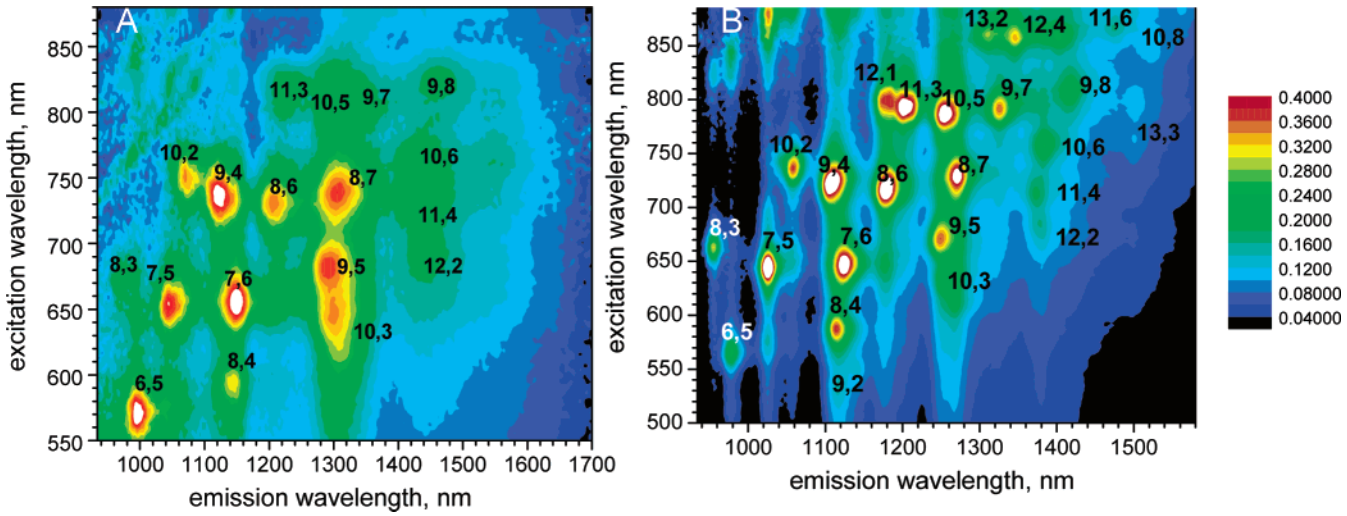

Figure 9. (A) Photoluminescence map (emission intensity vs excitation and emission wavelengths) of HiPCO nanotubes dispersed in NMP at a concentration of 0.006 mg/mL. (B) PL map of HiPCO SWNTs in NaDDBS/D_2O dispersion.

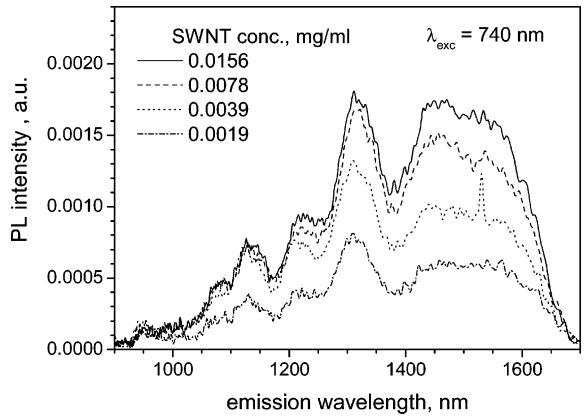

Figure 10. Typical concentration dependence of PL emission spectra for HiPCO SWNTs in NMP excited at 740 nm.

significantly red-shifted in NMP. This probably reflects a specific interaction of nanotubes with NMP molecules. The PL shifts correspond to the shifts of electronic transition energies E_{11} and E_{22} of $-(20 - 32)$ and $-(22 - 43)$ meV, respectively.

The number of distinct PL peaks assigned to different (n,m) nanotube species in Figure 9 is too small to draw statistically firm conclusions as to whether the PL shifts depend on the structure (helicity) of nanotubes and in what manner. However, there seems to be a clear trend for larger red shifts at increasing nanotube diameters (compare, for instance, (9,7) and (10,6) tubes ($d = 1.10$ and 1.11 nm, respectively) with (6,5) and (7,5) tubes ($d = 0.75$ and 0.83 nm, respectively) in Figure 9B). The origin of this diameter (nanotube curvature) effect is not clear at the moment.

PL emission spectra (excited at 740 nm) are shown in Figure 10 as a function of nanotube concentration. At each concentration the spectral shape is the same, indicating no changes in populations of individual nanotube types as the overall concentration is changed. However the PL intensity falls smoothly with concentration. The PL intensity of a given peak, I_{PL}, is proportional to the total number of individual nanotubes involved in that specific optical transition. As the spectral shape is unchanged with concentration, the intensity of the peak at 1320 nm, for example, is proportional to the total number of individual nanotubes in the sample and hence $I_{PL} \propto N_{ind}/V$. The intensity of this peak has been plotted as a function of concentration in Figure 7B and normalized to the AFM datum at $C_{NT} = 0.015$ mg/mL. Its concentration dependence matches the AFM data for N_{ind}/V almost perfectly. In addition, the PL intensity can be normalized to concentration and expressed as I_{PL}/C_{NT}. It can be easily shown that this quantity is proportional to the mass fraction of individual nanotubes: $I_{PL}/C_{NT} \propto M_{ind}/M_T$. The concentration-normalized PL intensity has been plotted in Figure 7C. Again its concentration dependence matches very well to the AFM data for M_{ind}/M_T. This shows categorically that the statistical data for populations of individual nanotubes as a function of concentration apply to the nanotubes in solution and not just after drying. This confirms that the concentration dependence of the bundle size distributions in situ is a real effect.

Note that the AFM measurements have been performed on freshly prepared NMP dispersions whereas the PL measurements have been delayed by 1−2 weeks. A further ultrasonic treatment was found to improve the PL intensity only ~2-fold at best, independent of the SWNT concentration. This suggests that the fraction of individually dispersed nanotubes is relatively stable within weeks at least in agreement with the AFM and sedimentation measurements. Interestingly, a concentration of individual nanotubes in water dispersions with the SDS, NaDDBS, or sodium cholate surfactant (considered as very efficient additives for dispersing SWNTs) appears to be also limited at a similar level of ~0.01 mg/mL, suggesting that similar debundling effects occur in these dispersions.

The PL of nanotubes dispersed in NMP, even at very low concentrations <0.005 mg/mL, is, by a factor of ~50−100, weaker compared to the water−surfactant dispersions of similar optical density at the excitation wavelength. According to the AFM, absorption, as well as the above PL data, this difference cannot be explained by a smaller fraction of individual (luminescent) nanotubes in NMP. (For well-prepared water−surfactant dispersions this fraction is assumed to be over 50%.[16,35]) Therefore we believe that the main reason for the weak PL is an intrinsically low PL efficiency for nanotubes when dispersed in NMP or a similar aromatic amine solvent due to solvent−nanotube interactions.

Finally, micro-Raman measurements of HiPCO nanotubes deposited on quartz substrates by spin-coating of NMP dispersions were carried out. These also show a significant fraction of individual nanotubes in the low-concentration dispersions. Figure 11 gives examples of Raman spectra recorded for substrate-deposited nanotubes. The spectra a and b show narrow, one-peak radial breathing mode (RBM) patterns that are

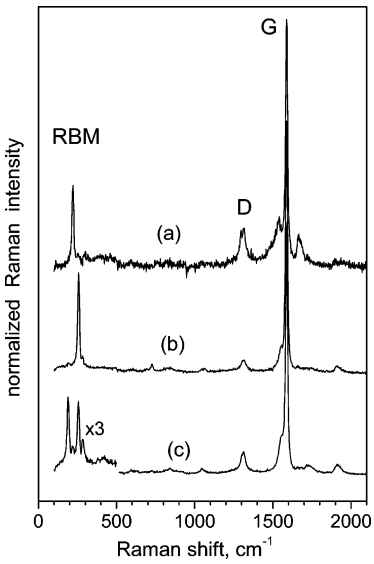

Figure 11. Raman spectra of nanotubes deposited from an NMP dispersion ($C = 0.008$ mg/mL) on a quartz substrate: (a,b) individual nanotubes assigned to (12,3) and (11,1) structures, respectively, and (c) a small nanotube bundle. The laser excitation wavelength is 633 nm. Indicated are two characteristic regions corresponding to the radial breathing and tangential G-mode vibrations.

consistent with individual nanotubes or at least small bundles with only one resonant tube type.[36] Nanotube-like objects showing two or more RBM features (similar to spectrum c in Figure 11) were also frequently found and assigned to small bundles of only a few nanotubes.

Discussion

It seems clear both from the work presented here and from the literature in general that nitrogen-containing solvents such as NMP are good dispersants for carbon nanotubes. However, this leads to the question as to which properties of these solvents are required for dispersion to occur. First it should be pointed out that, despite the casual use of the word "solution" in the literature, no direct evidence has ever been presented to show that carbon nanotubes are thermodynamically soluble in any binary system. However, whether the systems we are dealing with are solutions or dispersions, their properties will depend strongly on the magnitude (and sign) of the enthalpy of mixing. This parameter is a measure of the relevant strengths of solute−solute interactions versus solvent−solvent interactions versus solvent−solute interactions.[33] In colloidal dispersions the enthalpy of mixing tends to be positive, reflecting attractive, short-range intercolloid interactions. In true solutions the enthalpy of mixing tends to be slightly positive or even negative reflecting a more favorable solute−solvent interaction. In the case of macromolecular solutions the enthalpy of mixing, ΔH_{mix}, is given by[32]

$$\Delta H_{mix} = z\Delta E n_1 \phi_2 \tag{9}$$

where z is the coordination number, n_1 is the number of moles of solvent, and ϕ_2 is the macromolecule volume fraction. The parameter ΔE is given by

$$\Delta E = -(E_{11} + E_{22} - 2E_{12}) \tag{10}$$

where E_{11} is the solvent−solvent interaction energy, E_{22} is the solute−solute interaction energy, and E_{12} is the solute−solvent interaction energy. This means that the more negative E_{12} becomes the smaller ΔE and hence ΔH_{mix} become. Furthermore, if $|E_{12}| > (|E_{11}| + |E_{22}|)/2$, then ΔH_{mix} actually becomes negative. Thus, to successfully disperse carbon nanotubes in any solvent the solvent−nanotube interaction must be as strong as possible.

It has been pointed out by Ausman et al.[18] and subsequently by Landi et al.[22] and Furtado et al.[20] that all successful nanotube dispersing solvents are characterized by high electron pair donicity. This suggests that the presence of electron lone pairs, as for solvents such as NMP and DMF, results in weak solvent−nanotube charge transfer. This would certainly be expected to result in strong solvent nanotube binding. However, this condition alone is insufficient as dimethylsulfoxide (DMSO), a poor solvent for nanotubes, contains three lone pairs. Furtado[20] suggests that the dominant interaction is the adsorption of solvent molecules on the nanotube surface stabilized by the donation of π electrons from the nanotube to the solvent. Again this should result in strong solvent nanotube binding.

In addition Landi[22] has pointed out that the presence of alkyl groups attached to the carbonyl of amide solvents tends to stabilize the double bond character in the resonance-stabilized amide thus stabilizing the solvent molecules dipole moment. This, they suggest, results in a stronger solvent−nanotube interaction as shown by the higher observed dispersability of SWNTs in *N*,*N*-dimethylpropanamide (DMP) compared to that in DMF.[22] This suggests that the interaction may depend strongly on the dipole moment of the molecule. However, it should be pointed out that other highly polar molecules such as DMSO[18] and acetonitrile[22] do not disperse SWNTs. Landi[22] also suggest that π stacking of the solvent molecules on the sidewall of the nanotube may play a role in the solvent−nanotube interaction. They suggest that this interaction is optimized when solvent bond lengths and angles match the hexagonal structure of graphite. This however seems unlikely as the symmetry breaking due to the wall curvature precludes perfect lattice matching for molecules adsorbed at the van der Waals distance from the nanotube sidewall.[37]

It should not be forgotten that the concept of a perfectly hexagonal nanotube sidewall is an abstraction. All nanotubes contain defects even if the numbers are low. In addition purification of nanotubes by methods such as acid oxidation generally results in the covalent attachment of moieties such as carboxylic acid. Even after vacuum annealing one cannot be totally sure that the nanotubes contain only carbon. Thus, we cannot rule out the possibility that solvents interact preferentially with defects or possibly with polar functionalities and not with the hexagonal graphitic lattice.

Finally we must recognize that nonenthalpic factors can strongly effect nanotube dispersion. Consider a situation where strong solvent−nanotube interactions result in the solvent stacking on the nanotube sidewall in a partially ordered fashion. If the interfacial layers of solvent are ordered compared to the bulk solvent, then this will result in a reduction in solvent configurational entropy on mixing,[38] ΔS_O, where

$$\Delta S_O = \Delta S_{O,A} A \tag{11}$$

where $\Delta S_{O,A}$ is the reduction in configurational entropy per unit area and A is the nanotube−solvent interfacial area. This reduction in entropy is equivalent to an enthalpic cost of

$$\Delta H_O = -T\Delta S_{O,A} A > 0 \tag{12}$$

which increases as the interfacial area, A, increases. This means that it costs more and more energy to create the interface as

debundling proceeds. This energy cost is over and above that associated with the enthalpy of mixing. It has been shown that this effect can partly account for the insolubility of nanotubes in toluene.[38] This suggests that successful solvents do not actually π-stack on the nanotube sidewall as suggested by Landi.

Thus, it appears that the required characteristics for solvents to act as nanotube dispersants are large solvent−nanotube interaction energies relative to solvent−solvent and nanotube−nanotube interactions and the absence of ordering at the nanotube−solvent−nanotube interface. While most of the solvents described in the literature appear to display high lone pair donacity we cannot assume that this is indeed a prerequisite. We cannot rule out the possibility of the existence of strongly interacting but disordered solvents that do not display high lone pair donacity.

While the high lone pair donacity of NMP probably plays a role in the solvent−nanotube interaction, we can be certain that the total solvent−nanotube interaction has other contributions from London and dipole−induced dipole interactions, for example. In any case, it is certain that the total solvent−nanotube interaction energy must be high, resulting in a small (positive) or even negative enthalpy of mixing. In addition, as we know that NMP is a good dispersant, we can infer that there is no prohibitive configurational entropy penalty associated with the solvent−nanotube interface. This suggests that the interaction with the nanotube does not induce significant solvent ordering in the case of NMP.

Conclusions

In conclusion, using NMP we can routinely fabricate good quality SWNT dispersions without the need for ultracentrifugation. While at higher concentrations ($C_I > 0.02$ mg/mL) these dispersions contain some large aggregates, these can be removed by mild centrifugation. UV−vis−NIR absorbance spectroscopy can be used to monitor these dispersions before and after centrifugation. These measurements show that the absorption coefficient approaches 3500 mL $mg^{-1}m^{-1}$ at low concentrations with an average value of ~3250 mL mg^{-1} m^{-1} in the low-concentration regime. In addition the fractional aggregate concentration increases from close to zero at $C_I = 0.02$ mg/mL to almost 100% at $C_I = 0.1$ mg/mL.

Sedimentation and AFM measurements show that, after mild centrifugation, the dispersions are stable against both sedimentation and aggregation. AFM further shows that the bundle diameters tend to decrease with concentration until very small bundles are found at low concentrations. This can be explained by an equilibrium characterized by a maximum number density of bundles. This allows the calculation of the minimum solvent volume per bundle, which is very close to the volume of solvent enclosed by the sphere whose diameter is equal to the bundle length. This suggests that the bundle diameter distribution adjusts to the concentration such that the dispersion is always close to the dilute/semidilute boundary.

In addition, a population of individual nanotubes is present at all concentrations. The fraction of individual nanotubes increases as the concentration is decreased, approaching 70% at low concentration. We can also calculate the mass fraction of individual nanotubes, which tends to be 10% at low concentration. Two related quantities are the number density and mass density of individual nanotubes. These quantities are of course related and both display a maximum at approximately $C_{NT} \approx 0.01$ mg/mL. This is then the optimum concentration for finding individual nanotubes. The ratio of these quantities gives the average nanotube mass, which is concentration-independent as expected. The average nanotube mass is ~6.8 $\times 10^5$ g/mol, which corresponds to an average nanotube length of ~950 nm. The presence of individual nantoubes in NMP at different concentrations was confirmed by photoluminescence spectroscopy. Both the PL intensity and the ratio of PL intensity over concentration scaled with concentration in the same way as N_{ind}/V and M_{ind}/M_T as measured by AFM. This confirms that the AFM measurements are representative of the dispersion as a whole and not the drying phase. Finally, micro-Raman measurements carried out on spin-coated films confirm the presence of large quantities of individual nanotubes.

One important point can be made that applies to dispersions of all types of one-dimensional nanostructures. In many cases dispersions consisting solely of individual nanotubes are required. The standard procedure is to prepare a dispersion at reasonably high concentration and centrifuge to remove the bundles. However, our work shows that an optimum concentration exists with a maximum quantity of individual nanotubes. Thus, counter-intuitively, dispersions fabricated at this (lower) concentration and then centrifuged should have a higher concentration of individual nanotubes compared to those prepared at high concentrations. This can significantly increase the concentrations of dispersions of individual nanotubes available to researchers.

Acknowledgment. The authors acknowledge the support of the European Union in the form of the European Community's Human Potential Program under Contract No. HPRN-CT-2002-00192 (NANOTEMP). J.N.C. and W.J.B. also thank Science Foundation Ireland and the Irish Higher Educational Authority for financial support.

References and Notes

(1) Baughman, R. H.; Zakhidov, A. A.; de Heer, W. A. *Science* **2002**, *297*, 787.

(2) Yu, M.; Lourie, O.; Dyer, M. J.; Kelly, T. F.; Ruoff, R. S. *Science* **2000**, *287*, 637.

(3) Coleman, J. N.; Khan, U.; Gun'ko, Y. K. *Adv. Mater.* **2006**, *18*, 689.

(4) Wei, B. Q.; Vajtai, R.; Ajayan, P. M. *Appl. Phys. Lett.* **2001**, *79*, 1172.

(5) Kim, P.; Shi, L.; Majumdar, A.; McEuen, P. L. *Phys. Rev. Lett.* **2001**, *8721*.

(6) Nuriel, S.; Liu, L.; Barber, A. H.; Wagner, H. D. *Chem. Phys. Lett.* **2005**, *404*, 263.

(7) Kis, A.; Mihailovic, D.; Remskar, M.; Mrzel, A.; Jesih, A.; Piwonski, I.; Kulik, A. J.; Benoit, W.; Forro, L. *Adv. Mater.* **2003**, *15*, 733.

(8) Salvetat, J. P.; Briggs, G. A. D.; Bonard, J. M.; Bacsa, R. R.; Kulik, A. J.; Stockli, T.; Burnham, N. A.; Forro, L. *Phys. Rev. Lett.* **1999**, *82*, 944.

(9) Davis, V. A.; Ericson, L. M.; Parra-Vasquez, A. N. G.; Fan, H.; Wang, Y. H.; Prieto, V.; Longoria, J. A.; Ramesh, S.; Saini, R. K.; Kittrell, C.; Billups, W. E.; Adams, W. W.; Hauge, R. H.; Smalley, R. E.; Pasquali, M. *Macromolecules* **2004**, *37*, 154.

(10) Ramesh, S.; Ericson, L. M.; Davis, V. A.; Saini, R. K.; Kittrell, C.; Pasquali, M.; Billups, W. E.; Adams, W. W.; Hauge, R. H.; Smalley, R. E. *J. Phys. Chem. B* **2004**, *108*, 8794.

(11) Coleman, J. N.; Fleming, A.; Maier, S.; O'Flaherty, S.; Minett, A. I.; Ferreira, M. S.; Hutzler, S.; Blau, W. J. *J. Phys. Chem. B* **2004**, *108*, 3446.

(12) Dalton, A. B.; Stephan, C.; Coleman, J. N.; McCarthy, B.; Ajayan, P. M.; Lefrant, S.; Bernier, P.; Blau, W. J.; Byrne, H. J. *J. Phys. Chem. B* **2000**, *104*, 10012.

(13) McCarthy, B.; Coleman, J. N.; Curran, S. A.; Dalton, A. B.; Davey, A. P.; Konya, Z.; Fonseca, A.; Nagy, J. B.; Blau, W. J. *J. Mater. Sci. Lett.* **2000**, *19*, 2239.

(14) Murphy, R.; Coleman, J. N.; Cadek, M.; McCarthy, B.; Bent, M.; Drury, A.; Barklie, R. C.; Blau, W. J. *J. Phys. Chem. B* **2002**, *106*, 3087.

(15) Duesberg, G. S.; Burghard, M.; Muster, J.; Philipp, G.; Roth, S. *Chem. Commun.* **1998**, 435.

(16) O'Connell, M. J.; Bachilo, S. M.; Huffman, C. B.; Moore, V. C.; Strano, M. S.; Haroz, E. H.; Rialon, K. L.; Boul, P. J.; Noon, W. H.; Kittrell, C.; Ma, J. P.; Hauge, R. H.; Weisman, R. B.; Smalley, R. E. *Science* **2002**, *297*, 593.

(17) Blake, R.; Gun'ko, Y. K.; Coleman, J.; Cadek, M.; Fonseca, A.; Nagy, J. B.; Blau, W. J. *J. Am. Chem. Soc.* **2004**, *126*, 10226.

(18) Ausman, K. D.; Piner, R.; Lourie, O.; Ruoff, R. S.; Korobov, M. *J. Phys. Chem. B* **2000**, *104*, 8911.

(19) Bahr, J. L.; Mickelson, E. T.; Bronikowski, M. J.; Smalley, R. E.; Tour, J. M. *Chem. Commun.* **2001**, 193.

(20) Furtado, C. A.; Kim, U. J.; Gutierrez, H. R.; Pan, L.; Dickey, E. C.; Eklund, P. C. *J. Am. Chem. Soc.* **2004**, *126*, 6095.

(21) Krupke, R.; Hennrich, F.; Hampe, O.; Kappes, M. M. *J. Phys. Chem. B* **2003**, *107*, 5667.

(22) Landi, B. J.; Ruf, H. J.; Worman, J. J.; Raffaelle, R. P. *J. Phys. Chem. B* **2004**, *108*, 17089.

(23) Liu, J.; Casavant, M. J.; Cox, M.; Walters, D. A.; Boul, P.; Lu, W.; Rimberg, A. J.; Smith, K. A.; Colbert, D. T.; Smalley, R. E. *Chem. Phys. Lett.* **1999**, *303*, 125.

(24) Maeda, Y.; Kimura, S.; Hirashima, Y.; Kanda, M.; Lian, Y. F.; Wakahara, T.; Akasaka, T.; Hasegawa, T.; Tokumoto, H.; Shimizu, T.; Kataura, H.; Miyauchi, Y.; Maruyama, S.; Kobayashi, K.; Nagase, S. *J. Phys. Chem. B* **2004**, *108*, 18395.

(25) Umek, P.; Vrbanic, D.; Remskar, M.; Mertelj, T.; Venturini, P.; Pejovnik, S.; Mihailovic, D. *Carbon* **2002**, *40*, 2581.

(26) Lebedkin, S.; Arnold, K.; Hennrich, F.; Krupke, R.; Renker, B.; Kappes, M. M. *New J. Phys.* **2003**, *5*, 140.

(27) Hennrich, F.; Krupke, R.; Lebedkin, S.; Arnold, K.; Fischer, R.; Resasco, D. E.; Kappes, M. M. *J. Phys. Chem. B* **2005**, *109*, 10567.

(28) Lian, Y. F.; Maeda, Y.; Wakahara, T.; Akasaka, T.; Kazaoui, S.; Minami, N.; Choi, N.; Tokumoto, H. *J. Phys. Chem. B* **2003**, *107*, 12082.

(29) Nicolosi, V.; Vrbanic, D.; Mrzel, A.; McCauley, J.; O'Flaherty, S.; McGuinness, C.; Compagnini, G.; Mihailovic, D.; Blau, W. J.; Coleman, J. N. *J. Phys. Chem. B* **2005**, *109*, 7124.

(30) Nicolosi, V.; Vrbanic, D.; Mrzel, A.; McCauley, J.; O'Flaherty, S.; Mihailovic, D.; Blau, W. J.; Coleman, J. N. *Chem. Phys. Lett.* **2005**, *401*, 13.

(31) Coleman, J. N.; Blau, W. J.; Dalton, A. B.; Munoz, E.; Collins, S.; Kim, B. G.; Razal, J.; Selvidge, M.; Vieiro, G.; Baughman, R. H. *Appl. Phys. Lett.* **2003**, *82*, 1682.

(32) Donald, A. M.; Windle, A. H. *Liquid Crystalline Polymers*, 1st ed.; Cambridge University Press: Cambridge, U. K., 1992.

(33) Rubinstein, M.; Colby, R. H. *Polymer Physics*, 1st ed.; Oxford University Press: Oxford, U. K., 2003.

(34) Tucknott, R.; Yaliraki, S. N. *Chem. Phys.* **2002**, *281*, 455.

(35) Bachilo, S. M.; Strano, M. S.; Kittrell, C.; Hauge, R. H.; Smalley, R. E.; Weisman, R. B. *Science* **2002**, *298*, 2361.

(36) Duesberg, G. S.; Blau, W. J.; Byrne, H. J.; Muster, J.; Burghard, M.; Roth, S. *Chem. Phys. Lett.* **1999**, *310*, 8.

(37) Coleman, J. N.; Ferreira, M. S. *Appl. Phys. Lett.* **2004**, *84*, 798.

(38) Grujicic, M.; Cao, G.; Roy, W. N. *J. Mater. Sci.* **2004**, *39*, 2315.